Stiffness-Tunable Origami Structures via Multimaterial Three-Dimensional Printing

Article *in* Acta Mechanica Solida Sinica · June 2023

DOI: 10.1007/s10338-023-00403-1

7 authors, including:

Cheng Jianxiang
Southern University of Science and Technology
23 PUBLICATIONS **935** CITATIONS
SEE PROFILE

Honggeng Li
Southern University of Science and Technology
37 PUBLICATIONS **1,178** CITATIONS
SEE PROFILE

Bingcong Jian
Tongji University
21 PUBLICATIONS **328** CITATIONS
SEE PROFILE

Qi Ge
University of Colorado Boulder
103 PUBLICATIONS **9,506** CITATIONS
SEE PROFILE

Acta Mechanica Solida Sinica
https://doi.org/10.1007/s10338-023-00403-1

Stiffness-Tunable Origami Structures via Multimaterial Three-Dimensional Printing

Qingjiang Liu[1,2] · Haitao Ye[1,2] · Jianxiang Cheng[1,2] · Honggeng Li[1,2] · Xiangnan He[1,2] · Bingcong Jian[1,2] · Qi Ge[1,2]

Received: 22 February 2023 / Revised: 18 May 2023 / Accepted: 18 May 2023

Abstract
Origami structure has been employed in many engineering applications. However, there is currently no strategy that can systematically achieve stiffness-tunable origami (STO) structures through proper geometric design. Here, we report a strategy for designing and fabricating STO structures based on thick-panel origami using multimaterial 3D printing. By adjusting the soft hinge position, we tune the geometric parameter ψ to program the stiffness and strength of origami structures. We develop origami structures with graded stiffness and strength by stacking Kresling origami structures with different ψ. The printed structures show great cyclic characteristics and deformation ability. After optimizing combinations of structures with different ψ, the multi-layer Kresling STO structures can effectively reduce the peak impact, showing a good energy absorption effect. The proposed approach can be implemented in various origami patterns to design and tune the mechanical properties of origami structures for many potential applications.

Keywords Origami · Multimaterial 3D printing · Stiffness-tunable structure

1 Introduction

Origami is the ancient art of paper folding that can transform two-dimensional flat paper into a complex three-dimensional structure [1]. Thanks to the great deformability, large-storage ratio, high reconfigurability, easy assembly and diversified design space, origami structures have a wide range of applications in engineering fields [2, 3], such as robots [4, 5], flexible electronics [6], aerospace [7], flexible medical stents [8], civil engineering [9], and energy absorption structures [10]. Rigid origami is a subset of origami with stiff facets rotating around predetermined crease lines, and no deformation occurs on the facets [11]. In real-world designs, the thickness often cannot be neglected to grant stiffness to ensure its structural performance [12]. There are several strategies to preserve the kinematic properties with foldable thick-panel origami mechanisms [13, 14]. However, once the origami structures are fixed, the mechanical behavior of the structure is uniform, which cannot adapt to changeable loading conditions [15]. The tunable mechanical properties of materials and structures are essential for tuning motion [16], saving energy, and delivering high power [17, 18]. By tuning the different geometric parameters of the 2D pattern, different units with different stiffnesses can be combined to obtain mechanical metamaterials [15, 19] with graded stiffness [14]. Multi-stable [20, 21] and self-locking mechanisms [22–24] have also been used to tune structures. However, in most cases, the tunable mechanical properties of thick-panel origami are not compatible with foldability and deformability. In addition, thick-panel origami demands complicated manufacturing processes, which restricts further parameterization and functionalization of origami structures.

Three-dimensional printing (3D printing) is an emerging advanced manufacturing technology that creates complex 3D objects in free form, which potentially outperforms the limits of traditional methods [25]. Fused deposition modeling (FDM) 3D printing forms 3D structures by melting thermoplastic filament and extruding it through the printing nozzle to

✉ Bingcong Jian
jianbc@sustech.edu.cn

✉ Qi Ge
geq@sustech.edu.cn

[1] Shenzhen Key Laboratory of Soft Mechanics and Smart Manufacturing, Southern University of Science and Technology, Shenzhen 518055, China

[2] Department of Mechanical and Energy Engineering, Southern University of Science and Technology, Shenzhen 518055, China

Published online: 27 June 2023

generate patterns for each layer according to predetermined tool paths [26]. Compared with other 3D printing technologies, FDM 3D printing is the most widely used one due to its simplicity, inexpensiveness, and compatibility with various engineering plastics. Many attempts have been made to fabricate origami structures through FDM 3D printing [26, 27]. Compared with the past stamping and cutting manufacturing scheme, FDM 3D printing can realize parametric customized integrated manufacturing, which is also convenient for design modification and realization and can manufacture different patterns of origami metamaterials [28]. Because the deformation of origami structures can be regarded as stiff panels that rotate around predetermined hinges, FDM multimaterial 3D printing can make different parts of the structure composed of different materials to perform different functions, such as stiff panels and soft hinges. Therefore, FDM provides an option for the manufacture strategy to systematically achieve stiffness-tunable origami structures through proper geometric design.

Here, we report a strategy for designing and fabricating stiffness-tunable origami (STO) structures based on thick-panel origami using multimaterial 3D printing. By tuning the position of soft hinges at the joint of the stiff panel, the stiffness of origami structures with different patterns can be tuned systematically. We fabricate thick-panel origami structures based on zero-thickness origami patterns and tune the geometric parameter ψ to program the stiffness and strength. We develop structures with graded stiffness and strength by stacking origami structures based on the Kresling pattern with different ψ. Furthermore, the structures can withstand cyclic loading more than 100 times, exhibiting good cyclic characteristics and deformation ability. After optimizing and combining the structural layers with different ψ, six-layer Kresling STO structures can reduce the peak impact force from 640 to 66 N at the impact energy of 22 J. The proposed approach can be implemented in various origami patterns and can be utilized to design and tune the mechanical properties of origami structures for many potential applications.

2 Manufacturing and Design Approaches for STO Structures

Figure 1a illustrates the manufacturing process to fabricate the 2D flat pattern for an STO structure through a commercial FDM multimaterial 3D printer (Ultimaker S5, the Netherlands) with the resolution of 0.2 mm. As shown in Fig. 1b, the 2D flat pattern consists of stiff panels and soft hinges. In order to ensure robust interfacial bonding between them, the stiff panel is made up of a stiff material (i.e., polylactic acid—PLA) as the core, wrapped by a soft material (i.e., thermoplastic polyurethane—TPU) as the skin. The material properties of PLA and TPU are shown in Fig. S1. Since the soft material is continuous in both soft hinges and stiff panels, the two parts can be firmly bonded. As an example, Fig. 1c presents a printed planar Kresling origami pattern, which can be folded and attached at its two vertical ends to form a 3D Kresling origami structure (Fig. 1d). The Kresling origami structure consists of three layers exhibiting different stiffnesses. As shown in Fig. 1d, when a 3-kg dumbbell is placed on top of the origami structure, the top layer deforms the most and the bottom layer deforms the least, reflecting the stiffness difference in the three layers. The stiffness of each layer can be readily tuned by adjusting the design parameters.

Figure 1e illustrates a typical origami hinge with two stiff panels connected by one soft hinge. We can tune the stiffness of an origami hinge by changing the critical design parameter ratio ψ, which is defined as $\psi = h/l$, with h and l denoting the position and length of the soft hinge, respectively. When the soft hinge is in line with the inner side of the stiff panel, h is zero; when the soft hinge is in line with the outer side of the stiff panel, h equals to $t_\mathrm{p} - t_\mathrm{h}$, where t_p and t_h are the thicknesses of the stiff panel and soft hinge, respectively. To demonstrate the ψ -dependent stiffness, we printed five origami hinges with l set to be 2 mm and h varying from 0 to 2 mm. The experiments were conducted at a loading rate of 60 mm/min using the MTS machine (100 N load cell, USA). As shown in Fig. 1f, when ψ is small ($\psi = 0$ or 0.25), the soft hinge is close to the inner side of the stiff panel, and the stiffness of the origami hinge is nearly zero; when h gradually increases, the stiffness of the origami hinge rises drastically from 36 N/m ($\psi = 0.5$) to 281 N/m ($\psi = 1$). When ψ is different, the degree of interference between thick panels is different, and the tensile strain of soft hinges is different, resulting in a different growth rate of reaction force. The simulation of compression process of the sample with $\psi = 0.0$, 0.5, and 1.0 is shown in Fig. S2. Figure 1g and h present the snapshots of the folding processes for the origami hinges with $\psi = 0$ and 1, respectively, which explain the stiffness-enhancing mechanism with higher ψ. As shown in Fig. 1g, when $\psi = 0$, the hinge can fold easily, and the soft hinge deformation is small (32.9%). In Fig. 1h, when $\psi = 1$, the thickness of the stiff panels interferes with the folding process. In order to overcome the interference between the thick stiff panels, the soft hinge needs to be highly stretched (97.7%), which leads to a significant increase in the stiffness of the origami hinge.

3 Implementation of Stiffness-Tuning Approach to Various Origami Patterns

In Fig. 2, we implement the stiffness-tuning approach, which can adjust the origami stiffness by changing the design parameter ratio ψ to various origami patterns, including Kresling, Miura and Yoshimura. Figure 2a, d and g displays

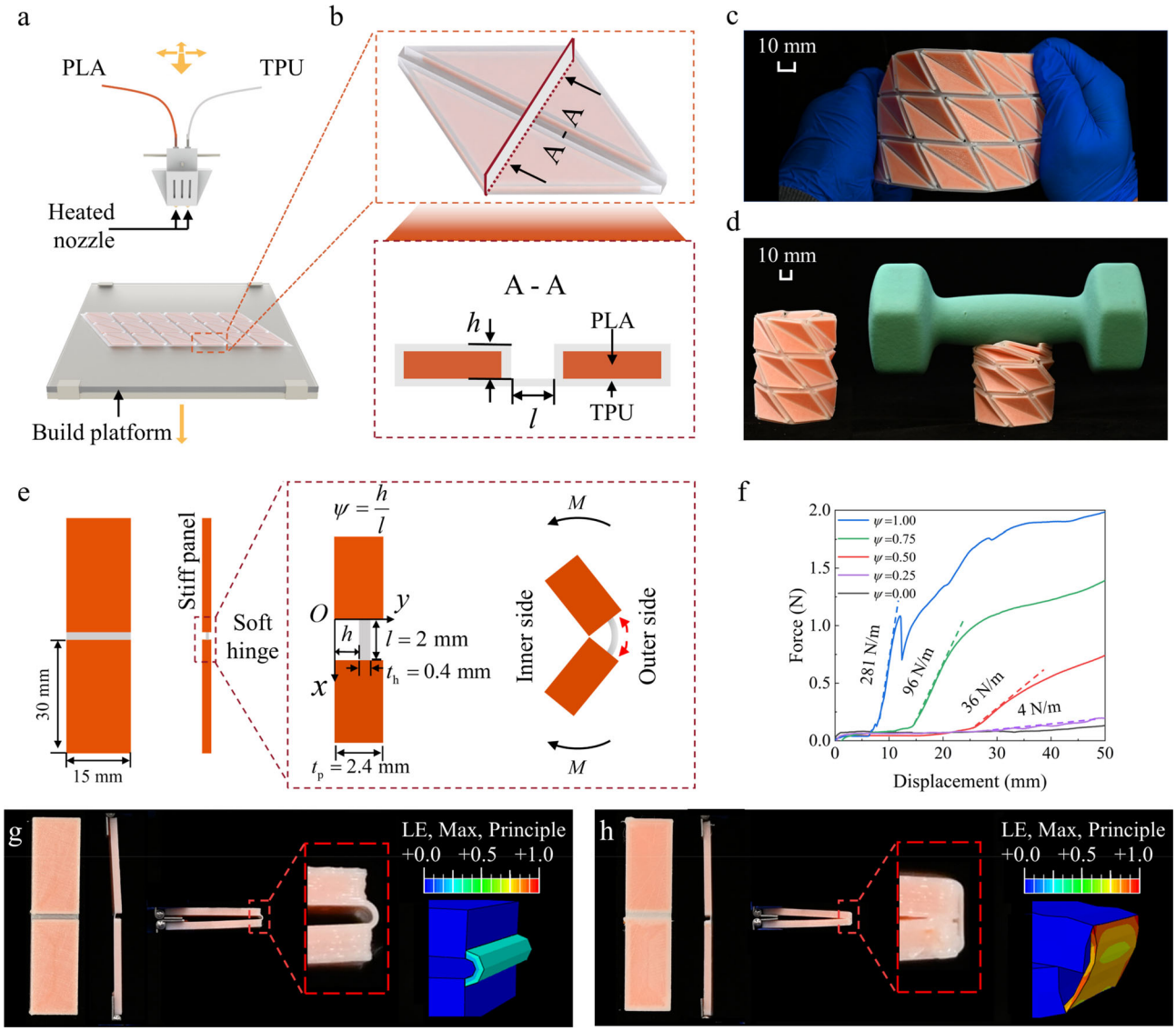

Fig. 1 Effect of soft hinge position on the mechanical properties of thick-panel origami. **a** Illustration of thick-panel origami fabrication through FDM multimaterial 3D printing. **b** Encapsulation-based 3D printing strategy for planar Kresling origami structure unit. **c** Fabrication and mechanical behavior of three-layer cylindrical Kresling origami structure. **d** Three-layer 3D Kresling origami structure. **e** Schematic illustration of geometric parameters of sample in uniaxial compression experiment. **f** The graded stiffness and strength due to ψ. **g** The folding process and finite element analysis of the sample when $\psi = 0.0$. **h** The folding process and finite element analysis of the sample when $\psi = 1.0$

the arrangements of soft hinges in each pattern, respectively. Among them, the soft hinges in red are changeable in ψ, while the soft hinges in blue have constant ψ. In an origami pattern, there are "mountain" and "valley" creases. Here, we use solid lines to indicate "mountain" creases and dashed lines to indicate "valley" creases of the soft hinges. In Fig. 2a, the blue soft hinge is a "mountain" crease with $\psi = 0$, and the soft hinge in red dashed line is a "valley" crease with tunable ψ. Figure 2b presents a multimaterial 3D printed Kresling origami structure composed of six identical thick-panel Kresling pattern units. To demonstrate the foldability of the Kresling origami even with thick-panel interference during the folding process, as shown in Figure 2c, we printed a Kresling origami, where we set $\psi = 1.0$ for the soft hinges at the "valley" creases, so that two stiff panels interfere with each other to prevent folding. The geometric parameter design diagram of planar Kresling origami structure with $\psi = 1.0$ is shown in Fig. S3. However, it can be seen from the uniaxial compression experiment in Fig. 2c that the high stretchability of the soft hinges overcomes the thick-panel interference and allows the origami structure to be fully folded. The simulation of compression process of the cylindrical Kresling origami structure with $\psi = 1.0$ is shown in Fig. S4.

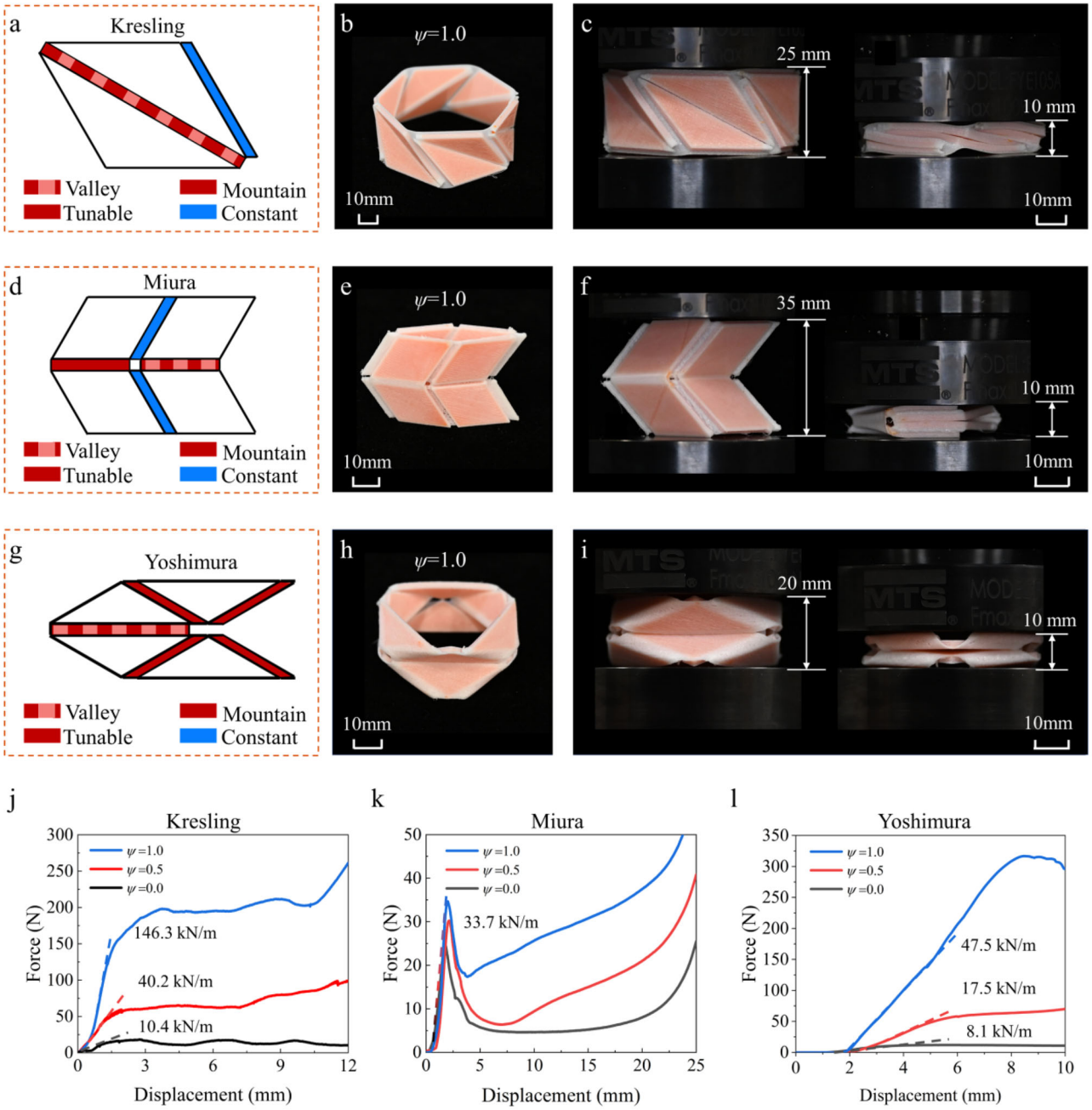

Fig. 2 The generalization of the effect of the position of the soft hinge on the mechanical properties of different thick-panel origami structures. **a** Kresling pattern. The the blue filled area denotes soft hinges with constant positions, while the red filled area represents flexible hinges whose positions can be changed. The spaced red filling indicates that the variable soft hinge is in the "valley" at this time, while the solid red filling indicates that the variable soft hinge is at the "mountain" at this time. The same rules apply to **d** and **g**. **b** The cylindrical origami structure is formed by folding the planar Kresling origami structure. **c** The compression process of the cylindrical Kresling origami structure. **d** Miura pattern. **e** The cylindrical origami structure of a combination of two-layer Miura planar origami structures. **f** Compression process of cylindrical Miura origami structure. **g** Yoshimura pattern. **h** The cylindrical origami structure is formed by folding the planar Yoshimura origami structure. **i** Compression process of cylindrical Yoshimura origami structure. **j-l** The relationship between force and displacement of cylindrical Kresling structure, cylindrical Miura origami structure, and cylindrical Yoshimura origami structure under different parameters

Similarly, as shown in Fig. 2d-i, we implement the stiffness-tuning approach to Miura- and Yoshimura-based origami structures. Figure 2d presents the arrangement of the soft hinges in the Miura origami pattern, and the legend is consistent with Fig. 2a. Figure 2e presents a fabricated Miura-based 3D origami structure consisting of two Miura units with tunable soft hinges ($\psi = 1.0$). As shown in Fig. 2f, the 3D Miura origami structure also exhibits great foldability even when the thick panels interfere with each other during folding. Figure 2g shows the soft hinge arrangement for the Yoshimura pattern where all the soft hinges are tunable in ψ. Figure 2h presents a fabricated Yoshimura-based 3D origami structure consisting of three Yoshimura units with $\psi = 1.0$ in all the tunable soft hinges. The foldability of the Yoshimura origami structure is validated in Fig. 2i.

In Fig. 2j–l, we conducted uniaxial compression tests to investigate the effect of ψ on the 3D origami structures based on Kresling, Miura, and Yoshimura patterns. We used MTS Model 43 for the quasi-static uniaxial compression at 2 mm/min. As shown in Fig. 2j, after changing ψ from 0 to 1, the stiffness of the Kresling-based origami structure measured at the linear region of the force–displacement curve increases from 10.4 kN/m to 146.3 kN/m. In Fig. 2k, the stiffnesses of the three Miura-based origami structures with different ψ values are nearly the same, and the increase in ψ only leads to the increase in the "yielding point" where the force starts to drop suddenly. The structural stiffness at 0–2.5 mm is caused by the Miura pattern itself. For the Yoshimura-based origami structures, the forces start to rise when the displacements are greater than 2 mm; the stiffness measured at the linear region of the force–displacement curve increases from 8.1 kN/m to 47.5 kN/m as ψ increases from 0 to 1. The reaction force of Yoshimura structures remains small when the displacement is smaller than 2 mm because of the 1-mm TPU at the upper and lower ends of the structure. Compared with Miura- and Yoshimura-based origami structures, Kresling-based origami structures exhibit higher sensitivity to the variation of ψ. Therefore, in the following of this manuscript, we use Kresling-based origami structures to investigate the stiffness tuneability through static and impact experiments. Unless otherwise stated, each layer of the following Kresling origami structures contains six units.

4 Static Response of Kresling STO Structure with Multiple Layers

The multimaterial 3D printing of STO structures endows origami structures with high design and manufacturing flexibility. As a result, we can easily design and fabricate multi-layer STO structures with different stiffnesses for each layer. As illustrated in Fig. 3a, we designed a three-layer Kresling STO structure with the ψ values of 0.5, 0.75 and 1.0 from top to bottom. In Fig. 3b, we conducted the compression test on such a printed three-layer STO structure. It can be seen that the top layer was folded first since its ψ value and stiffness were lowest; the bottom layer was folded last since its ψ value and stiffness were highest. As shown in Fig. 3c, we can further design and fabricate three-layer Kresling STO structures with different combinations of ψ values. Detailed combinations of ψ values are shown in Table 1. When the displacement ranged from 0 to 15 mm, Structures 2–4 had the same force–displacement curve as they had the same ψ value for the top layer ($\psi_1 = 0.25$). After 15-mm displacement, the stiffness of Structure 2 was higher than that of Structure 3 or 4 as the ψ value for the middle layer of Structure 2 ($\psi_2 = 0.75$) was greater than that of Structure 3 or 4 ($\psi_2 = 0.5$). After 30-mm displacement, Structure 3 exhibited a higher stiffness than Structure 4 as it had a higher ψ value for the bottom layer. Structure 1 had the highest stiffness across all displacement ranges because it had the highest ψ_1 in the displacement range 0–15 mm, the highest $\psi_1 + \psi_2$ in the displacement range of 15–30 mm, and the highest $\psi_1 + \psi_2 + \psi_3 (\psi_{\text{total}} = \psi_1 + \psi_2 + \psi_3)$ in the displacement range of 30–50 mm.

5 Cyclic Response of Kresling STO Structure with Multiple Layers

Mechanical repeatability during cyclic loading is desired for origami structures. However, many origami structures cannot undergo cyclic loading due to the plastic deformation on hinges or buckling on panels. In this work, the high stretchability and mechanical repeatability of the TPU material that forms the soft hinges endow the printed STO structures with excellent mechanical repeatability. As shown in Fig. 4a, we conducted cyclic loading–unloading tests on a single-layer Kresling STO structure with $\psi = 0$. The initial height of the structure was 25 mm, which reduced to 10 mm when fully folded. Figure 4b shows that the STO structure can undergo cyclic compression for more than 100 cycles. The force–displacement curve for the STO structure with $\psi = 0$ during cyclic loading is shown in Fig. 4b. A slight residual displacement (0.57 mm) can be found after 10 cycles of compression.

Figure 4c presents the relationship between residual displacement and the number of cycles for the STO structure with $\psi = 0$, 0.5 and 1.0, respectively. The residual displacement after the first cycle increases from 0 to 3.5 mm when the ψ value increases from 0 to 1. This can be attributed to two reasons: (i) as the ψ value increases, the soft hinges need to be stretched more to overcome the interference between stiff panels during folding; (ii) as shown in Fig. 4d, the TPU material forming the soft hinges exhibits apparent residual strain after the first cycle of stretching, and the magnitude of the residual strain is proportional to the maximum strain

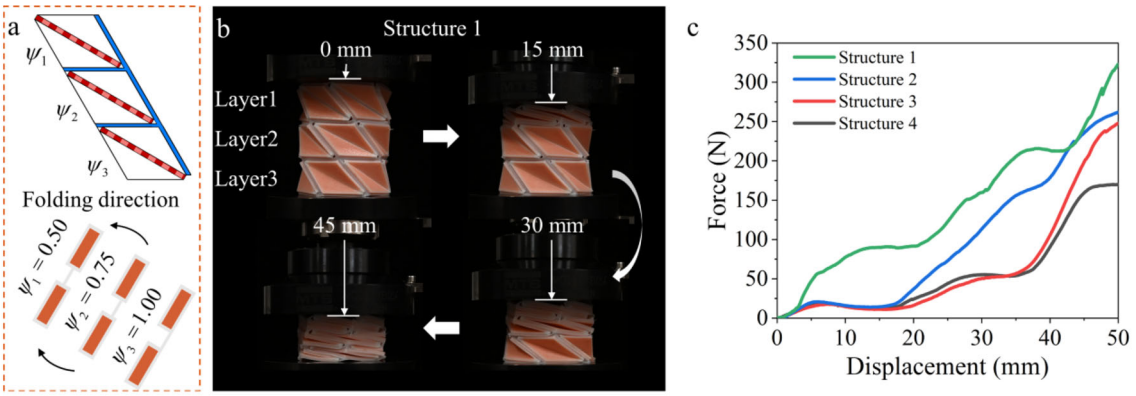

Fig. 3 Display of the graded stiffness of the three-layer cylindrical Kresling origami structure. **a** Schematic diagram of the cross section of the three-layer planar Kresling origami structure combination and the soft hinges. **b** The compression process of Structure 1 of the three-layer combination structure. **c** Graded stiffness display of the three-layer cylindrical Kresling origami structure

Table 1 Parameters ψ of three-layer cylindrical Kresling origami structures

Structure	ψ_1	ψ_2	ψ_3	ψ_{total}
1	0.50	0.75	1.00	2.25
2	0.25	0.75	1.00	2.00
3	0.25	0.50	1.00	1.75
4	0.25	0.50	0.75	1.50

in the loading cycle. Therefore, the high residual displacement in the STO structure with $\psi = 0.5$ or $\psi = 1.0$ results from the residual strain of the soft TPU hinge. In Fig. 4c, the residual displacement for the three STO structures slightly increases when the cyclic loading tests proceed after the first loading cycle, which is consistent with the observation from the cyclic loading tests for TPU materials where the residual strain also slightly increases after the first loading cycle. For further analysis and verification, we performed ten sets of cyclic loading test of the TPU material at 10%, 50%, and 100% strain, respectively, as shown in Fig. 4e. The results show that the first cycle with different strain values has a large residual strain compared to other cycles, consistent with the results in Fig. 4b and d. The dimension of the TPU specimen is shown in Fig. S5.

Besides single-layer STO structures, multi-layer STO structures exhibit excellent mechanical repeatability under cyclic loading. Figure 5a presents a three-layer STO structure where the ψ values from top to bottom are 0.5, 0.75, and 1, respectively. When the displacement of 15 mm was applied five times, only the top layer was repeatedly folded for five times, while the other two layers remained unfolded; when the cyclic displacement increased to 30 mm, both the top and middle layers were repeatedly folded; when the displacement rose to 45 mm, all three layers could be cyclically folded. Figure 5b shows the displacement input for the cyclic loading test. Figure 5c provides the force response, which indicates that the STO structure exhibits excellent mechanical repeatability.

Moreover, we also examined the mechanical repeatability of four-layer STO structures. To clearly illustrate the effect of ψ in different combinations of cylindrical Kresling origami structure units, we created Table 2. As shown in Fig. 5d, when a cyclic displacement of 30 mm was applied, the top two layers of Structure 5 ($\psi_1 = \psi_2 = 0.5$) were folded; when the displacement increased to 60 mm, not only the top two layers but also the bottom two layers ($\psi_3 = \psi_4 = 1.0$) were folded. Figure 5e shows the displacement input for the cyclic loading test of Structure 5–7. Figure 5f provides the force response, which illustrates that as the ψ_{total} value increases, a greater force is required to compress the same distance. It also indicates that the ψ value is related to the stiffness of the multi-layer Kresling origami structures.

6 Impact Experiment

Our design strategy endows thick-panel origami structures with designable and tunable stiffness and strength. The combination of different structural units can realize the complex force–displacement curve of graded stiffness. In this way, the two contradictory characteristics of high and low Young's moduli can be combined in a single structure. Moreover, the folding and deformation ability of the origami structure

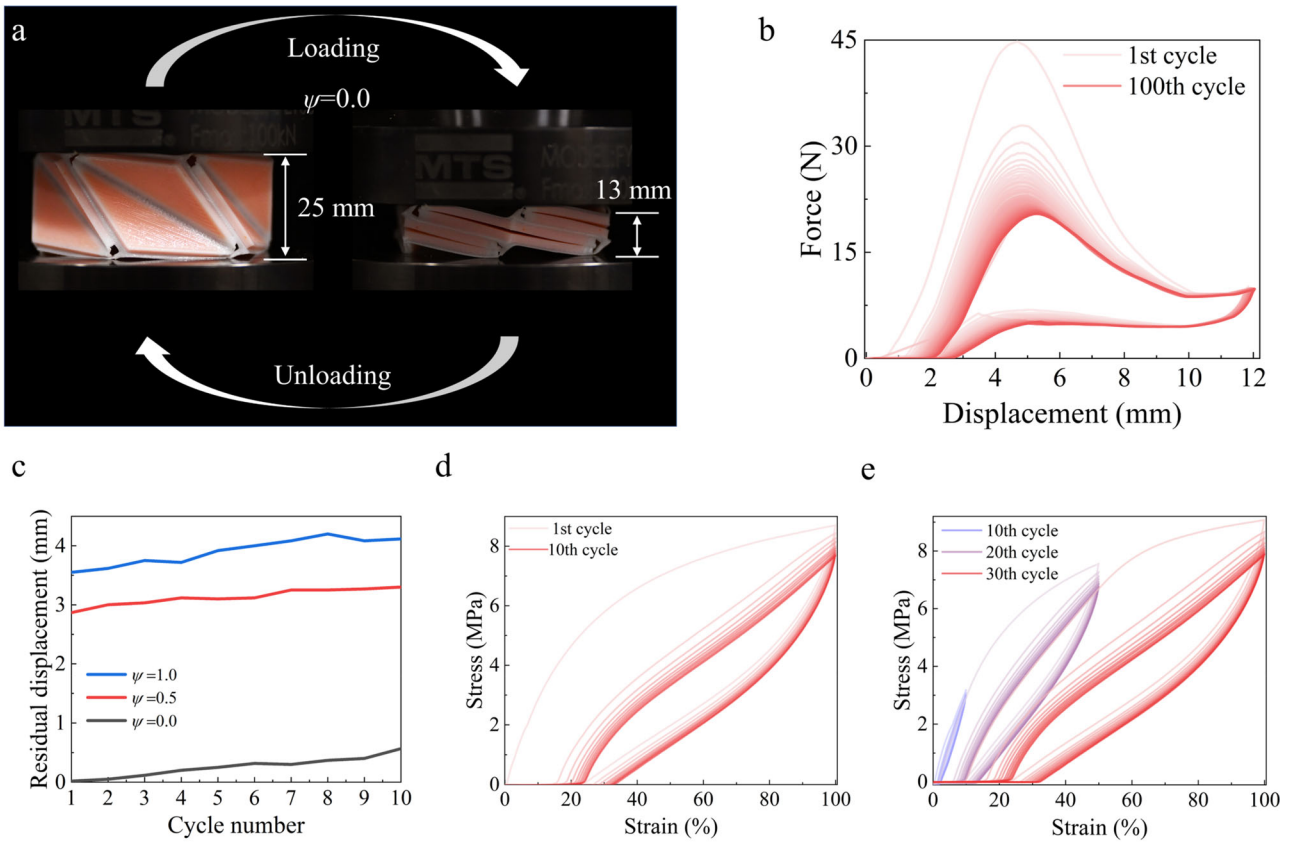

Fig. 4 Cyclic performance of the single-layer cylindrical Kresling origami structures and TPU material. **a** Schematic diagram of the cyclic loading experiment of the single-layer cylindrical Kresling origami structure with $\psi = 0.0$. **b** The relationship between the force and displacement of single-layer cylindrical Kresling origami structure with $\psi = 0.0$. **c** The relationship between the residual displacement and the number of cycles of the single-layer cylindrical Kresling origami structures with different ψ. **d** Cyclic compression results of the TPU material under 100% compressive strain. **e** Gradient loading–unloading results of the TPU material

provides it with large compressive displacement and deformation space during the compression process, resulting in increased contact time and improved energy absorption.

To verify that our design strategy provides the structure with good energy-absorbing performance, we assembled a set of impact test equipment, as shown in Fig. 6a. The equipment consists of two slide rails, with a flat plate carrying the weight m that moves up and down along them. The cylindrical Kresling origami structure is located directly above the platform, and the force sensor is under the platform. A high-speed camera is pointed directly at the structure and is responsible for capturing the deformation process. The impact energy can be adjusted by tuning weight m and height h, and is calculated as $E = mgh$. The weights we used weighed 8.25 kg, and when the impact heights were 270 mm and 210 mm to the platform, the energy of the two different impact heights were 22 J and 17 J, respectively. For each impact energy, 7 trials were performed, with Ct representing the control trial without the origami structure for energy absorption. Table 3 displays the other 6 trials with different ψ_i combinations of six-layer cylindrical Kresling origami structures. Figure 6b shows the relationship between force and time under 22-J energy. From Fig. 6b, we can see that there are obviously multiple rebound phenomena in the control test. Moreover, the maximum contact reaction force is 640 N, which is the highest value. Structure 10 (S10) and Structure 12 (S12) are significantly lower than others, and the order of magnitude is close to the size of the noise. Zooming in on the region from 0 to 90 ms, we obtain Fig. 6c. We counted the force received by the sensor under different energy impacts in 7 tests. It is shown in Fig. 6c that S10 and S12 can reduce the maximum force after impact to 10.3% (66/640) and 12.2% (78/640) of the control test, respectively. S10 is composed of six layers of $\psi = 1.0$ cylindrical Kresling origami structural units, and S12 is composed of one layer of $\psi = 0.0$, two layers of $\psi = 0.5$, and three layers of $\psi = 1.0$. Figure 6d shows the maximum force of 7 trials under impacts of 17-J energy and 21-J energy. Compared with the control trials, all the other six groups of structures exhibited a significant energy absorption effect. The results indicate that S10 and S12 had the best energy absorption effect under each condition, while S11 and

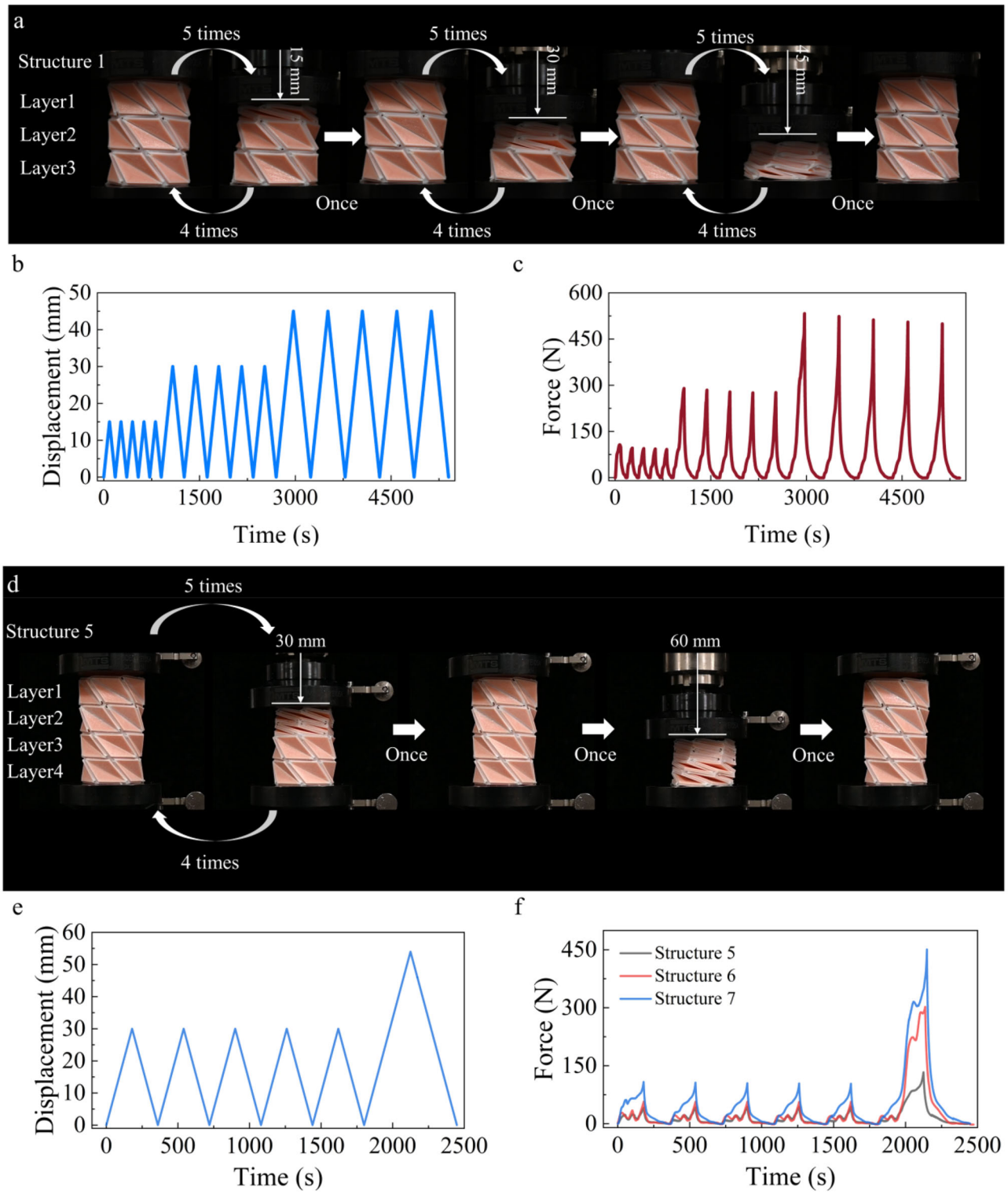

Fig. 5 The cyclic performance of the complex cylindrical Kresling origami structure with multi-layers of different cylindrical Kresling origami structural unit combinations. **a** Schematic diagram of the cyclic experiment for the three-layer cylindrical Kresling origami structure with different combinations of units. **b-c** Displacement–time and force–time relationships of cyclic experiments for the three-layer cylindrical Kresling Origami structure combinations. **d** Schematic diagram of the cyclic experiment for four-layer cylindrical Kresling origami structure. **e–f** Displacement–time and force–time relationships of cyclic experiments for the four-layer cylindrical Kresling origami structure

Table 2 Parameters ψ of four-layer cylindrical Kresling origami structuers

Structure	ψ_1	ψ_2	ψ_3	ψ_4	ψ_{total}
5	0.5	0.5	1.0	1.0	3.0
6	0.0	0.0	1.0	1.0	2.0
7	0.0	0.0	0.5	0.5	1.0

S13 also showed a great energy absorption effect under the impact of 17 J, they were slightly inferior under 22 J.

From the high-speed camera image in Fig. 6e, we can find that S10 buckled at 20 ms, followed by obvious failure damage at 40 ms, and the second impact contact at 155 ms, during which part of the stiff plate of the structure fell off. It ended up holding the weight consistently after 265 ms since it eventually failed. For S12, the structure of different layers was folded sequentially. The energy was absorbed by the stretching of TPU. The structure was fully compressed at 40 ms, and did not fail. At 155 ms, the structure completely returned to its original state and remained vertical. Finally, after 265 ms, the gradient deformation was always maintained due to the effect of ψ. In our strategy of changing the value of ψ, the six-layer cylindrical Kresling origami structure exhibited a great energy absorption effect. After combining structural units with different ψ, the structure can not only have the good energy-absorbing effect, but also have the characteristics of reusability, which is not available in most energy-absorbing materials.

7 Conclusion

In summary, we report a universal design and fabrication approach for stiffness-tunable origami structures based on thick-panel Kresling origami to achieve both graded stiffness and superior energy absorption performance. Specifically, we use a multimaterial FDM 3D printing and wrapping strategy to fabricate structures and tune the position of soft hinges, so that the printed origami structures have different stiffness. We have demonstrated both experimentally and numerically that the graded structure is able to generate multi-level graded stiffness, which can be tuned through its geometric parameters. We have studied the mechanism behind the varying stiffness of structures with different ψ and found that soft hinges made up of TPU are stretched to different strains during the same compressive displacement. By comparing the relationship between force and displacement of different single-layer cylindrical origami structures based on different patterns with different ψ under uniaxial compression, we have found that cylindrical Kresling origami structures exhibit higher sensitivity to the variation of ψ. By fabricating three-layer Kresling STO structures with different combinations of ψ values, it can be seen that the top layer is folded first since its ψ value and stiffness are lowest; while the bottom layer is folded last as its ψ value and stiffness are greatest. By tuning the ψ values, we can further tune the stiffness. In addition, the structures can withstand cyclic loading more than 100 times since the deformation concentrates on the soft hinge, which is made up of TPU with good cyclic characteristics and deformation ability. Finally, we have demonstrated that tuning the ψ values endows the 3D single-layer cylindrical Kresling STO structure with different stiffnesses. Furthermore, by combining six-layer Kresling STO structures with well-arranged ψ, the structure is endowed with superior capability to absorb impact energy, which can significantly reduce the impact peak force from 640 to 66 N and avoid secondary impact under the impact energy of 22 J. This design strategy for thick-panel origami can systematically tune the stiffness while retaining the native folding behavior of the origami pattern, which can be utilized in practical engineering applications.

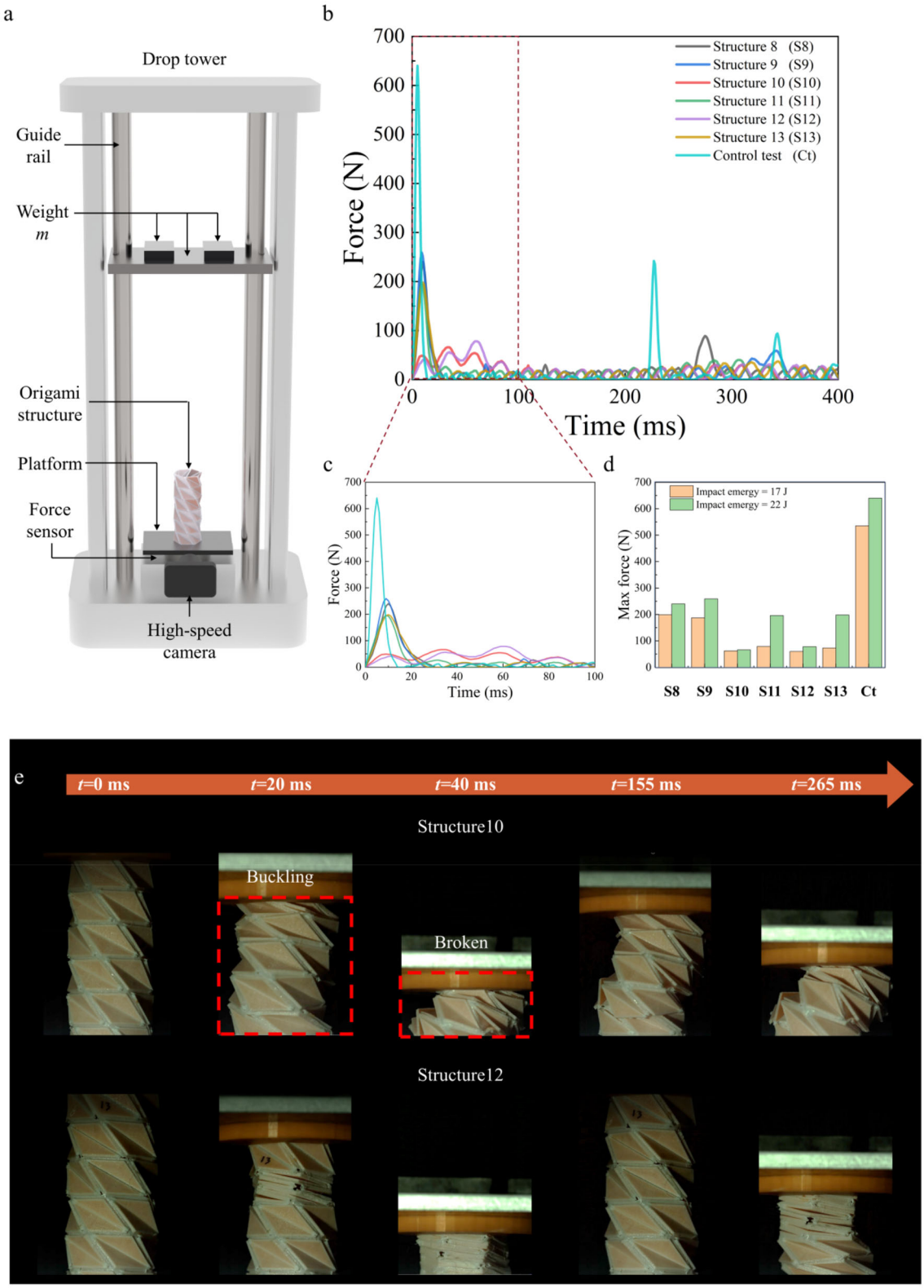

Fig. 6 Impact performance of the six-layer cylindrical Kresling origami structures. **a** Schematic diagram of the impact test equipment. **b**-**c** Force–time diagram of the impact test at 22-J energy. **d** The maximum impact force received by the sensor with different structures under different impact energies. **e** The deformation processes of Structure 10 and Structure 12 in the impact tests

Table 3 Parameters ψ of six-layer cylindrical Kresling origami structuers

Structure	ψ_1	ψ_2	ψ_3	ψ_4	ψ_5	ψ_6	ψ_{total}
8	0.0	0.0	0.0	0.0	0.0	0.0	0.0
9	0.5	0.5	0.5	0.5	0.5	0.5	3.0
10	1.0	1.0	1.0	1.0	1.0	1.0	6.0
11	1.0	0.5	0.5	0.0	0.0	0.0	2.0
12	0.0	0.5	0.5	1.0	1.0	1.0	4.0
13	0.0	1.0	1.0	0.5	0.5	0.5	3.5

Supplementary Information The online version contains supplementary material available at https://doi.org/10.1007/s10338-023-00403-1.

Acknowledgements This work is financially supported by the National Key Research and Development Program of China (2020YFB1312900), the National Natural Science Foundation of China (No. 12072142), the Key Talent Recruitment Program of Guangdong Province (No. 2019QN01Z438), and the Science Technology and Innovation Commission of Shenzhen Municipality (ZDSYS20210623092005017).

Author Contributions QL, HY, BJ and QG conceived the project and designed the research; QL and HY conducted experiments; QL performed FEM simulations. JC, HL, XH and BJ helped the experiments; QL and QG drafted manuscript; QL, BJ and QG revised manuscript.

Declarations

Conflict of interest The authors declare that they have no conflicts of interest.

Ethical Approval This study does not involve any sensitive information, and there are no ethical issues.

References

1. Lang RJ. The science of origami. Phys World. 2007;20(2):30–1.
2. Morris E, McAdams DA, Malak R, editors. The state of the art of origami-inspired products: A review. International Design Engineering Technical Conferences and Computers and Information in Engineering Conference; 2016: American Society of Mechanical Engineers.
3. Peraza-Hernandez EA, Hartl DJ, Malak RJ, Lagoudas DC. Origami-inspired active structures: a synthesis and review. Smart Mater Struct. 2014;23(9):094001.
4. Rus D, Tolley MT. Design, fabrication and control of origami robots. Nat Rev Mater. 2018;3(6):101–12.
5. Arun S, Anveeth B, Majumder A, editors. Advancements in Origami Inspired Robots, a Review. 2019 2nd International Conference on Intelligent Computing, Instrumentation and Control Technologies (ICICICT); 2019: IEEE.
6. Qi Z, Zhou M, Li Y, Xia Z, Huo W, Huang X. Reconfigurable flexible electronics driven by origami magnetic membranes. Adv Mater Technol. 2021;6(4):2001124.
7. Morgan J, Magleby SP, Howell LL. An approach to designing origami-adapted aerospace mechanisms. J Mech Des. 2016;138(5):052301–10.
8. Kuribayashi K, Tsuchiya K, You Z, Tomus D, Umemoto M, Ito T, et al. Self-deployable origami stent grafts as a biomedical application of Ni-rich TiNi shape memory alloy foil. Mater Sci Eng A. 2006;419(1–2):131–7.
9. Reis PM, Lopez Jimenez F, Marthelot J. Transforming architectures inspired by origami. Proc Natl Acad Sci. 2015;112(40):12234–5.
10. Ma J, You Z. Energy absorption of thin-walled square tubes with a prefolded origami pattern—part I: geometry and numerical simulation. J Appl Mech. 2014;81(1):011003–11.
11. Tachi T. Rigid-foldable thick origami. Origami. 2011;5(5):253–64.
12. Chen Y, Peng R, You Z. Origami of thick panels. Science. 2015;349(6246):396–400.
13. Lang RJ, Tolman KA, Crampton EB, Magleby SP, Howell LL. A review of thickness-accommodation techniques in origami-inspired engineering. Appl Mech Rev. 2018;70(1):010805–20.
14. Ma J, Song J, Chen Y. An origami-inspired structure with graded stiffness. Int J Mech Sci. 2018;136:134–42.
15. Zhai Z, Wang Y, Jiang H. Origami-inspired, on-demand deployable and collapsible mechanical metamaterials with tunable stiffness. Proc Natl Acad Sci. 2018;115(9):2032–7.
16. Mintchev S, Shintake J, Floreano D. Bioinspired dual-stiffness origami. Sci Robot. 2018;3(20):eaau0275.
17. Zhai Z, Wang Y, Lin K, Wu L, Jiang H. In situ stiffness manipulation using elegant curved origami. Sci Adv. 2020;6(47):eabe2000.
18. Wang Y, Li L, Hofmann D, Andrade JE, Daraio C. Structured fabrics with tunable mechanical properties. Nature. 2021;596(7871):238–43.
19. You Z. Folding structures out of flat materials. Science. 2014;345(6197):623–4.
20. Wo Z, Filipov ET. Stiffening multi-stable origami tubes by outward popping of creases. Extreme Mech Lett. 2023;58:101941–2016.
21. Melancon D, Forte AE, Kamp LM, Gorissen B, Bertoldi K. Inflatable origami: multimodal deformation via multistability. Adv Func Mater. 2022;32(35):2201891.
22. Jamalimehr A, Mirzajanzadeh M, Akbarzadeh A, Pasini D. Rigidly flat-foldable class of lockable origami-inspired metamaterials with topological stiff states. Nat Commun. 2022;13(1):1816.
23. Fang H, Chu SCA, Xia Y, Wang KW. Programmable self-locking origami mechanical metamaterials. Adv Mater. 2018;30(15):1706311.
24. Ye H, Liu Q, Cheng J, Li H, Jian B, Wang R, et al. Multimaterial 3D printed self-locking thick-panel origami metamaterials. Nat Commun. 2023;14(1):1607.

25. Gibson I, Rosen DW, Stucker B, Khorasani M. Additive manufacturing technologies. Berlin: Springer; 2021.
26. Van Manen T, Janbaz S, Zadpoor AA. Programming 2D/3D shape-shifting with hobbyist 3D printers. Mater Horiz. 2017;4(6):1064–9.
27. Mehrpouya M, Azizi A, Janbaz S, Gisario A. Investigation on the functionality of thermoresponsive origami structures. Adv Eng Mater. 2020;22(8):2000296.
28. Van Manen T, Janbaz S, Jansen KMB, Zadpoor AA. 4D printing of reconfigurable metamaterials and devices. Commun Mater. 2021;2(1):00165–8.